γ' precipitates with a twin orientation relationship to their hosting grain in a γ-γ' nickel-based superalloy

Suzanne Vernier, Jean-Michel Franchet, Christian Dumont, Philippe Vennegues, Nathalie Bozzolo

γ' precipitates with a twin orientation relationship to their hosting grain in a γ-γ' nickel-based superalloy

Suzanne Vernier[a,b*], Jean-Michel Franchet[b], Christian Dumont[c], Philippe Vennéguès[d] and Nathalie Bozzolo[a]

[a] MINES ParisTech, PSL – Research University, CEMEF – Centre de mise en forme des matériaux, CNRS UMR 7635, 1 rue Claude Daunesse, 06904 Sophia Antipolis, France
[b] Safran SA, Safran Tech – Materials & Process Department, 1 Rue Geneviève Aubé, 78114 Magny-les-Hameaux, France
[c] Aubert & Duval, Département R&D transformations, BP1, 63 770 Les Ancizes, France
[d] CRHEA-CNRS, UPR 10, rue Bernard Grégory, 06560 Valbonne, France

*Corresponding author. suzanne.vernier@mines-paristech.fr

Abstract

In a polycrystalline γ-γ' nickel-based superalloy, γ' precipitates with a close-to-twin orientation relationship to their surrounding matrix (named T-type precipitates) are found in recrystallized grains located near specific unrecrystallized grains (named recovered grains). This type of γ/γ' interface has not been reported in literature before. Inherited from the ingot conversion process, recovered grains are characterized by a high density of micrometric and close-to-coherent γ' precipitates. Resulting from the interaction of the recrystallization front with the latter precipitates, the T-type precipitates appear to form onto the recrystallization front. The present paper details the crystallographic characteristics of the T-type precipitates.

Keywords

Gamma - Gamma Prime nickel-based superalloy, Interphase boundary, Twin boundary, Recrystallization.

Polycrystalline γ-γ' nickel-based superalloys are commonly used to manufacture aircraft engine rotative parts due to their good mechanical behavior at high temperature (tensile, fatigue, creep resistance) [1]. Parts are usually derived from cast ingots through forging sequences [2,3]. They are made of a γ matrix in which γ' precipitates of various sizes are distributed. Both γ and γ' phases have a cubic structure but, while the γ phase is a Face Centered Cubic (FCC) non-ordered solid solution, the γ'-Ni_3(Al,Ti) phase has a $L1_2$ ordered structure. Yet, the mechanical properties of the alloy do not only depend on the size and spatial distribution of the precipitates [4], but also on the γ/γ' interface characteristics [5,6]. Indeed, γ' precipitates are reported in literature as coherent, semi-coherent or incoherent to their surrounding matrix [7]. Coherency means that the γ and γ' crystal lattices perfectly coincide at the γ/γ' interface. This is made possible by a low lattice parameter mismatch between the γ and γ' phases [8]. Coherent γ/γ' interfaces have very low energies [9,10] and form during the cooling stages of the forging process for example. However, if some misfit dislocations pile up at the γ/γ' interface, the lattice matching is only partial and the interface is semi-coherent [7]. Semi-coherency occurs when external stresses (high temperature plastic deformation) or internal stresses (e.g. induced by long aging treatments leading to particle coarsening) generate dislocation loops which are incorporated into the γ/γ' interface as misfit dislocations [11]. Finally, when there is no crystal lattice matching, the γ/γ' interface is incoherent and has a high energy [9]. Secondary γ' precipitates which form during the cooling stages of the forming process, are coherent with a cube-cube orientation relationship: they evolve from spheres to {100} bounded cubes as their size and/or the lattice misfit increase [12]. On the other hand, primary γ' precipitates, derived from the as-cast microstructure and high temperature billet forging sequences, are usually incoherent with no special orientation relationship, excepted in case of heteroepitaxial recrystallization where primary precipitates are found coherent with an orientation very close to that of their surrounding matrix [13–15]. The present work points out another type of γ/γ' interface which, to the best knowledge of the authors, has not been reported in literature before: γ' precipitates with a close-to-twin orientation relationship to their surrounding γ matrix have been evidenced. Those precipitates will be called T-type precipitates below. Close-to-twin means that the two γ and γ' cubic crystallographic cells are related by a misorientation close to, but a few degrees off, the theoretical 60° rotation around a common <111> axis. The Δθ tolerance which has been used to detect the T-type precipitates applies both to the 60° rotation angle and the <111> rotation axis, and amounts to 8.66° following Brandon's criterion for FCC twin boundaries [16]. T-type precipitates fall into this 8.66° tolerance and only very few of them strictly fulfills the perfect 60°<111>, which implies that the considered γ/γ' interfaces must be regarded as incoherent. T-type precipitates are found in some recrystallized grains next to

unrecrystallized grains characterized by a high density of micrometric close-to-coherent precipitates and called recovered grains. The present paper details the crystallographic characteristics of the T-type precipitates. The AD730^{TM} nickel-based superalloy whose composition is Ni-15.7Cr-8.5Co-4.0Fe-3.4Ti-3.1Mo-2.7W-2.25Al-1.1Nb-0.01B-0.015C-0.03Zr (wt.%) [17] is studied. Samples are cut out from an AD730^{TM} billet which contains elongated unrecrystallized grains typical of many cast-and-wrought heavily-alloyed γ/γ' nickel-based superalloys [18–20]. These grains are inherited from the ingot conversion process and characterized by a high density of intragranular precipitates. The samples were compressed at a sub-solvus temperature then solution-treated for 4 hours at 1080°C. The γ' solvus temperature of the alloy is about 1110°C. Longitudinal sample cross-sections were ground with Si papers and polished with diamond suspensions down to 1µm. Finally, to obtain a suitable surface quality for EBSD, samples were polished either by electropolishing (CH_3OH-10%$HClO_4$) or with a 0.02µm colloidal silica solution on a vibratory machine. Some samples also underwent a deeper electrolytic etching (HNO_3-45%H_2SO_4-13%H_3PO_4) to selectively dissolve the matrix and bring the γ' precipitates more into relief. SEM observations were carried out with a Zeiss Supra40 FEG-SEM operated at 15kV. The microscope is equipped with the QUANTAX EDS/EBSD system, from the Bruker Company, which is composed of an EDS XFlash 5030 detector and an e$^-$Flash^{HR} EBSD detector, both controlled by the ESPRIT® software package. Some EBSD data post-treatments were performed using MTEX, a freely available Matlab toolbox [21]. A TEM thin foil was lifted out of a region of interest using a Zeiss Crossbeam 550 FIB-SEM, equipped with an Oxford Instruments Symmetry EBSD detector which was used to perform Transmission Kikuchi Diffraction analyses (TKD) at 30 kV. Finally, TEM observations were performed with a JEOL 2100 FEG-TEM operated at 200 kV.

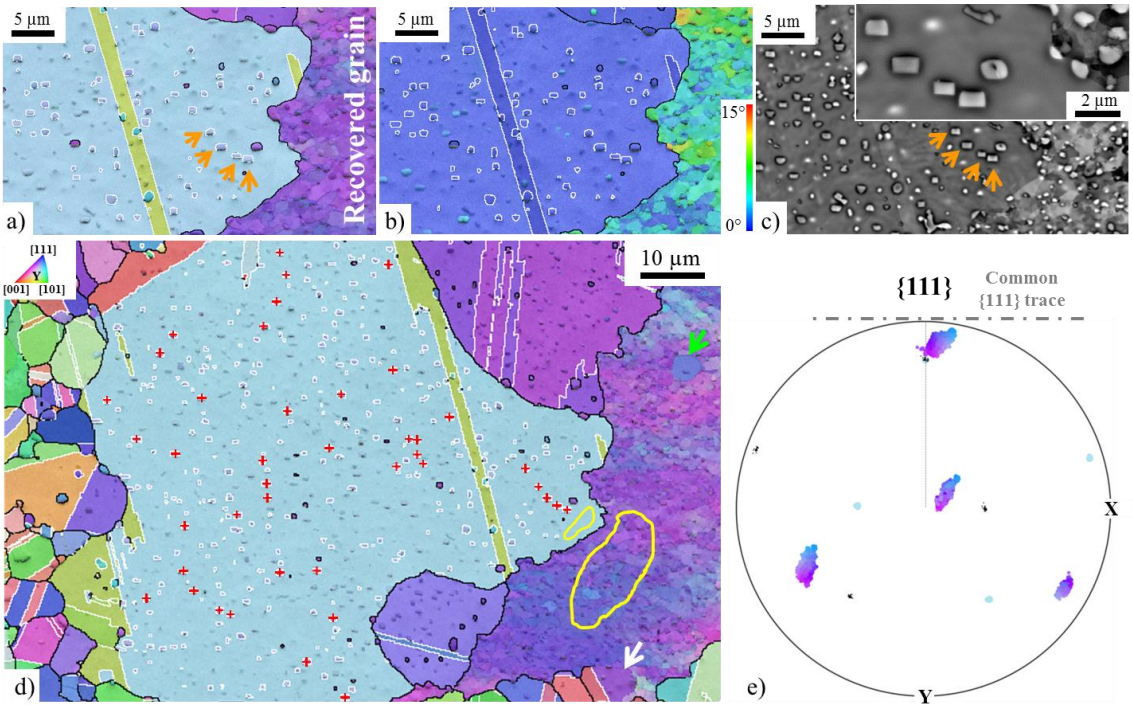

Figure 1. γ' precipitates with a twin orientation relationship to the matrix observed after static recrystallization. a) and d) Orientation overlaid on the band contrast map, grain boundaries plotted black (misorientation angle threshold: 10°) and twin boundaries (60°<111> with 8.66° tolerance, following Brandon's criterion [16]*) plotted white. The green and white arrows highlight HERX and CRX respectively. b) Misorientation angle to the mean grain orientation overlaid on the band contrast map. c) Backscattered electron images, where γ' precipitates appear bright despite their lower atomic number because of topographic effects induced by electropolishing. Orange arrows show examples of γ' precipitates with a twin orientation relationship to the matrix. e) {111} pole figure. Orientations of T-type precipitates (red crosses in d)) are plotted black; those of the matrix and the recovered grain (yellow selections in d)) are plotted with the same color as displayed in d). The dashed line is the {111} plane trace common to the T-type precipitates and the matrix.*

The samples present some areas where the recrystallized grain size is much larger than anywhere else. Those large recrystallized grains are located next to elongated unrecrystallized grains (Figure 1). These unrecrystallized grains show a high density of micrometric close-to-coherent precipitates and quite well-defined recovery cells; they will henceforth be called recovered grains. Here, the large recrystallized grains, which appeared during the solution treatment, have extensively grown inside the recovered grain to consume the stored strain energy. The large recrystallized grains exhibit numerous intragranular particles, many of them having a twin orientation

relationship to their hosting grain, within the tolerance given by Brandon's criterion (white boundaries in Figure 1). These particles with a close-to-twin orientation relationship, and called T-type precipitates in the following, were proved to be γ' precipitates considering two points. First, their chemical composition is rich in Ni, Ti and Al, and close to that of the primary precipitates (Table 1). Their chemical composition is also very similar to that of the precipitates inside the recovered grains (Table 1). The fact that primary precipitates are most likely formed at higher temperature than the precipitates of the recovered grains can account for the slight differences in composition. Then, the TEM diffraction pattern of a T-type precipitate shows superstructure spots confirming a $L1_2$ ordered structure whose cubic lattice parameter is very close to that of the non-ordered matrix (Figure 4).

Table 1. Chemical composition (wt. %) of T-type precipitates (T), precipitates inside recovered grains (R) and primary precipitates (P). EDS measurements performed at 15 kV.

γ'	Ni	Fe	Co	Cr	Mo	W	Al	Ti	Nb
T	70.9	1.8	5.6	5.5	0.8	0.7	4.2	9.2	1.3
R	70.4	2.0	5.7	6.1	0.9	0.6	4.1	8.9	1.3
P	73.0	1.5	5.0	3.3	0.4	0.4	4.6	10.3	1.5

Several arguments demonstrate that T-type precipitates are not the precipitates of the recovered grain which have been simply bypassed by the recrystallization front. They do originate from a specific mechanism and the T-type precipitate visible on the recrystallization front in Figure 2.b (blue arrow) underlines that this mechanism occurs at the recrystallization front. The first argument is that many T-type precipitates are larger than the close-to-coherent precipitates of the recovered grain. Second, while the precipitates of the recovered grain appear round in the sample section, T-type precipitates display rectangular shapes parallel to each other in Figures 1.c and 2.a. On the deep-etched sample (Figure 3), rectangular shapes are clearly visible for precipitates identified in recrystallized grains near recovered grains, their straight sides suggesting that they may be delimited by simple crystallographic planes. Finally, the orientations of the T-type precipitates appear more homogeneous than that of the recovered grain (and so of the close-to-coherent precipitates of the recovered grain) yet selected over a much smaller area (Figure 1.e/2.c).

Each time, the recrystallized grain hosting T-type precipitates shows a <111> axis close to those of the recovered grain it consumes (Figures 1.d and 2.c/e). The two recrystallization mechanisms occurring in the recovered grains can explain how such a common <111> axis is obtained. The first recrystallization mechanism is the Continuous Recrystallization (CRX), which means that cells resulting from the fragmentation of the grain under deformation recover and become new recrystallized grains once they are sufficiently misoriented with the surrounding matrix [22] (white arrow in Figure 1.d). The second mechanism is the HeteroEpitaxial Recrystallization (HERX) [13–15]: some γ' precipitates inside the recovered grain become surrounded by a coherent γ envelop of same crystalline orientation, this γ envelop can then grow in the hardened matrix as a new recrystallized grain (green arrow in Figure 1.d). For both recrystallization mechanisms, the newly recrystallized grains have orientations which are close to that of the nearby recovered grain, and consequently have all four <111> axes initially close to those of the recovered grain. Then, when growing inside the recovered grain, the newly recrystallized grains can twin (60°<111>) due to a growth accident at the recrystallization front [23,24]. The obtained twin crystals still have one <111> axis close to those of the recovered grain.
From the {111} pole figures (Figures 1.d and 2.c/e), the <111> axis common to the recrystallized and recovered grains is also the <111> axis around which the T-type precipitates are rotated compared to their surrounding matrix. Thus, that <111> axis is in fact common to the three orientations: T-type precipitates, recrystallized and recovered grains. Moreover, when the T-type precipitates appear rectangular in the sample section, the longest sides of their rectangular shape coincide with the corresponding common {111} plane trace. This strongly suggests that T-type precipitates might be bounded by {111} planes. The TEM thin foil gives additional information about the 3D shape of the T-type precipitates since it was milled perpendicular to a plane in which T-type precipitates appeared rectangular (Figure 2.a). As the T-type precipitates appear now round in the thin foil (Figure 2.d), it can be concluded that T-type precipitates are micrometric plate-like particles bounded by {111} planes on their flat sides.

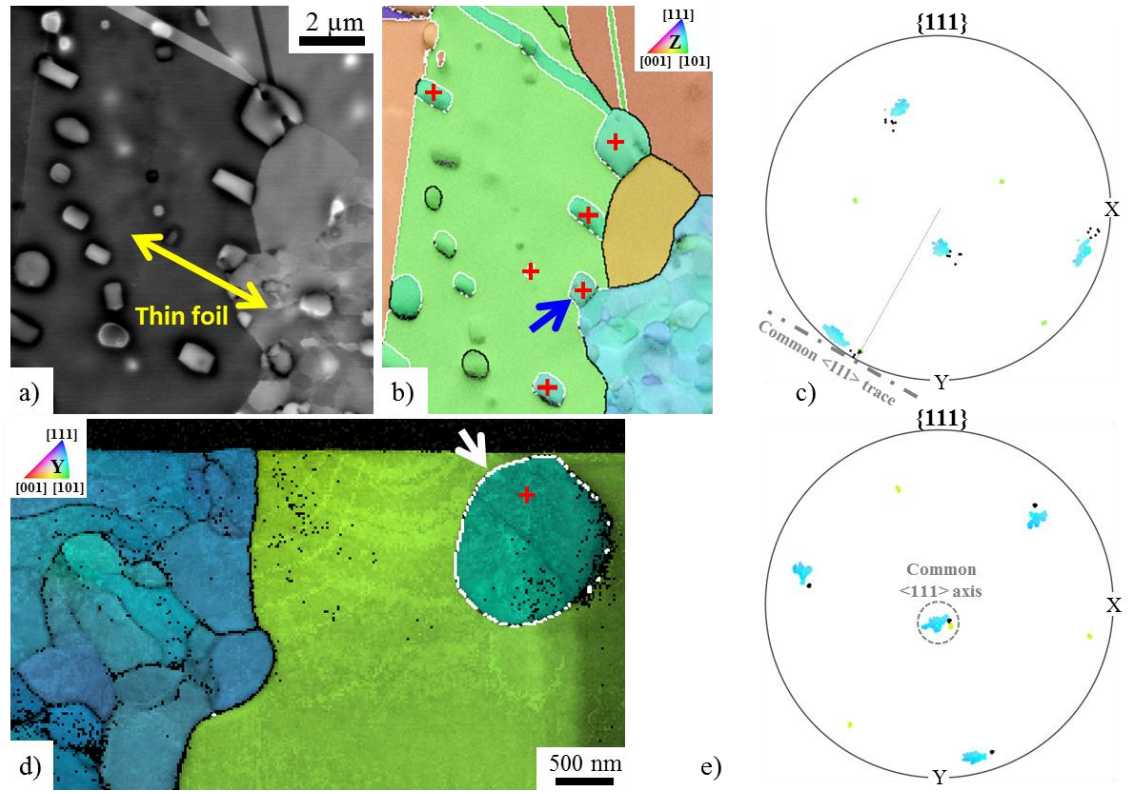

Figure 2. Another example of T-type precipitates observed after static recrystallization. a) Backscattered electron image. b) Orientation overlaid on the band contrast map, grain boundaries (misorientation angle threshold: 10°) plotted black and twin boundaries (60°<111> with 8.66° tolerance) plotted white. c) and e) {111} pole figures. Orientations of the T-type precipitates (red crosses in b) and d)) are plotted black; those of the matrix and the recovered grain are plotted with the same color as displayed in b) and d). In c) the dashed line is the {111} plane trace common to the T-type precipitates and the matrix. d) TKD performed on the TEM thin foil lifted out of the region displayed in a): Orientation overlaid on the band contrast map, grain boundaries plotted black and twin boundaries plotted white. The white arrow highlights a T-type precipitate.

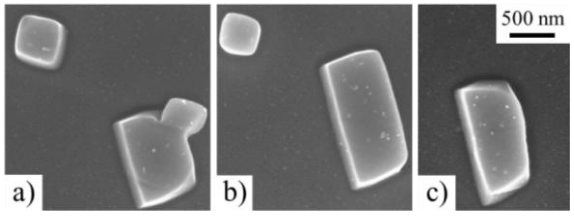

Figure 3. Images of precipitates found in statically recrystallized grains near recovered grains. Secondary electrons, electrolytic etching.

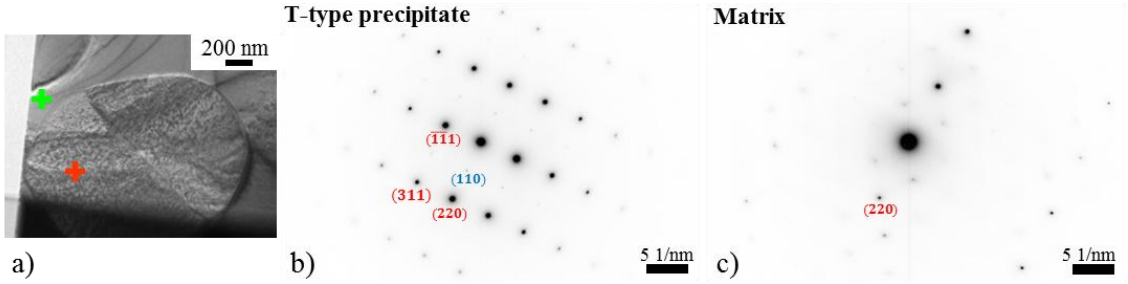

Figure 4. TEM characterization of the T-type precipitate in Figure 2.d). a) Multi-beam image. b) and c) Diffraction patterns of the T-type precipitate ([$\bar{1}$12] zone axis; red cross area in a)) and of the surrounding matrix (green cross area in a)). Superstructure spots such as (110) are visible on the T-type precipitate diffraction pattern.

To the best knowledge of the authors, γ/γ' twin boundaries in nickel-based superalloys have not been reported yet. In austenitic steels, Vaughan [25] pointed out the nucleation of plate-shaped $M_{23}C_6$ carbides in twin orientation relationship to the matrix at incoherent twin boundaries and some Σ9 boundaries. Vaughan explained the twin orientation relationship by two points: i) the morphology of these specific boundaries; ii) the good atomic fit between the {111} $M_{23}C_6$ planes and the {111} matrix planes. In fact, incoherent twin boundaries and some Σ9 boundaries exhibit small coherent {111} facets which allow the carbides, by nucleating on these facets, to grow with a twin orientation relationship to the matrix. Like the γ and γ' phases, austenite and $M_{23}C_6$ carbides have a cubic crystal structure. So, even if the context is different, Vaughan's results seem interesting to consider, as it was shown that T-type precipitates form at the recrystallization front and that recrystallized and recovered grains share a <111> axis.

Regarding the possible impact of such T-type precipitates on the alloy properties, it can be reminded that γ/γ twin boundaries localize large amounts of dislocations under cyclic loading due to the elastic incompatibility stresses between twin and matrix [26]. This dislocation concentration is deleterious for the properties of the alloy in case of large twin boundaries. However, here the γ/γ' twin-like interface area per precipitate is small, and the T-type precipitates are only observed occasionally near recovered grains. Thus, it is quite unlikely that T-type precipitates could have a significant impact on the macroscopic behaviour of the material. Nevertheless this question deserves further investigations given the criticality of the aircraft engine rotative parts.

In summary, the present work evidences twin-like interfaces between γ' precipitates and their hosting γ grain. Precipitates 60°<111> rotated to their matrix within the 8.66° tolerance given by Brandon's criterion (T-type precipitates) were found in the AD730^{TM} polycrystalline nickel-based superalloy after static recrystallization of some recovered areas. They are located in large recrystallized grains which have grown inside recovered grains. T-type precipitates are plate-like particles bounded by {111} planes on their flat sides. The <111> axis corresponding to these planes is a <111> axis common to the T-type precipitates, their hosting grain and the consumed recovered grain. Indeed, the hosting grain has a <111> axis very close to those of the recovered grain because it results from the CRX or HERX of the recovered grain and subsequent annealing twinning events. T-type precipitates originate from the precipitates of the recovered grain that the recrystallization front has to overcome. However the sizes, the orientation spread and the morphology of the T-type precipitates prove that they have not been simply bypassed by the recrystallization front but that they form according a specific mechanism on the recrystallization front. The details of this mechanism will be the purpose of future research.

Acknowledgments

This work has been carried out thanks to the financial support of the ANR-Safran industrial chair OPALE. The authors acknowledge J. Cormier (Institute Pprime, Futuroscope-Chasseneuil, France) for this help in optimizing sample etching. The authors also acknowledge S. Schädler (Zeiss microscopy customer center Europe, Oberkochen, Germany) and H. Mansour (Oxford Instruments, Gometz la Ville, France) for the FIB preparation of the TEM thin foil and the TKD analyses.

References

[1] R.C. Reed, The Superalloys, Fundamentals and Applications, Cambridge University Press, 2006.

[2] D. Furrer, H. Fecht, JOM 51 (1999) 14–17.

[3] T.M. Pollock, S. Tin, J. Propuls. Power 22 (2006) 361–374.

[4] M.P. Jackson, R.C. Reed, Mater. Sci. Eng. A 259 (1999) 85–97.

[5] D.A. Grose, G.S. Ansell, Met. Trans. A 12 (1981) 1631–1645.

[6] J.M. Oblak, D.F. Paulonis, D.S. Duvall, Metall. Trans. 5 (1974) 143–153.

[7] F.C. Campbell, Elements of Metallurgy and Engineering Alloys, ASM International, 2008.

[8] M. V. Nathal, R.A. Mackay, R.G. Garlick, Mater. Sci. Eng. 75 (1985) 195–205.

[9] V. Randle, B. Ralph, Acta Metall. 34 (1986) 891–898.

[10] G.S. Rohrer, J. Mater. Sci. (2011) 5881–5895.

[11] A.K. Singh, N. Louat, K. Sadananda, Metall. Trans. A 19 (1988) 2965–2973.

[12] R.A. Ricks, A.J. Porter, R.C. Ecob, Acta Metall. 31 (1983) 43–53.

[13] M.A. Charpagne, T. Billot, J.M. Franchet, N. Bozzolo, J. Alloys Compd. 688 (2016) 685–694.

[14] M. Charpagne, T. Billot, J. Franchet, N. Bozzolo, Superalloys 2016 (2016) 417–426.

[15] M.A. Charpagne, P. Vennéguès, T. Billot, J.M. Franchet, N. Bozzolo, J. Microsc. 263 (2016) 106–112.

[16] D.G. Brandon, Acta Metall. 14 (1966) 1479–1484.

[17] A. Devaux, B. Picqué, M.F. Gervais, E. Georges, T. Poulain, P. Héritier, Superalloys 2012 (2012) 911–919.

[18] B.J. Bond, C.M.O. Brien, J.L. Russell, J.A. Heaney, M.L. Lasonde, 8th Int. Symp. Superalloy 718 Deriv. (2014) 107–118.

[19] C. Crozet, A. Devaux, R. Forestier, S. Charmond, M. Hueller, D. Helm, W. Buchmann, Superalloys 2016 Proc. 13th Int. Symp. Superalloys (2016) 437–446.

[20] R.S. Minisandram, L.A. Jackman, J.L. Russell, M.L. Lasonde, J.A. Heaney, A.M. Powell, 8th Int. Symp. Superalloy 718 Deriv. (2014) 95–105.

[21] G. Nolze, R. Hielscher, J. Appl. Crystallogr. 49 (2016) 1786–1802.

[22] J. Humphreys, G.S. Rohrer, A. Rollett, Recrystallization and Related Annealing Phenomena, 3rd ed., Elsevier Ltd, 2017.

[23] Y. Jin, B. Lin, M. Bernacki, G.S. Rohrer, A.D. Rollett, N. Bozzolo, Mater. Sci. Eng. A 597 (2014) 295–303.

[24] Y. Jin, B. Lin, A.D. Rollett, G.S. Rohrer, M. Bernacki, N. Bozzolo, J. Mater. Sci. 50 (2015) 5191–5203.

[25] D. Vaughan, Philos. Mag. 25 (1972) 281–290.

[26] J. Miao, T.M. Pollock, J. Wayne Jones, Acta Mater. 57 (2009) 5964–5974.